JOURNAL OF PROPULSION AND POWER
Vol. 26, No. 5, September–October 2010

Effects of Magnetohydrodynamic Interaction-Zone Position on Shock-Wave/Boundary-Layer Interaction

Wei-Yi Su*
Nanjing University of Aeronautics and Astronautics, 210016 Nanjing, People's Republic of China
Xin-Yu Chang†
Chinese Academy of Sciences, 100190 Beijing, People's Republic of China
and
Kun-Yuan Zhang‡
Nanjing University of Aeronautics and Astronautics, 210016 Nanjing, People's Republic of China

DOI: 10.2514/1.49838

A third-order weighted essentially nonoscillatory and non-free-parameter difference scheme magnetohydrodynamic solver has been established to investigate the mechanisms of magnetohydrodynamics controlling separation induced by an oblique shock wave impinging on a flat plate. The effects of magnetohydrodynamic interaction-zone location on the separation point, reattachment point, separation-bubble size, and boundary-layer velocity profiles are analyzed. The results show that there exists a best location for the magnetohydrodynamic zone to be applied, where the separation point is delayed the farthest, and the separation bubble is decreased up to about 50% in size compared to the case without magnetohydrodynamic control, which demonstrated the promising of magnetohydrodynamics suppressing the separation induced by shock-wave/boundary-layer interactions.

Nomenclature

B_i	=	magnetic field component in i direction
E_z	=	electric field in z direction
e_t	=	total energy
$\mathbf{F}$, $\mathbf{G}$	=	inviscid flux
$\mathbf{F_v}$, $\mathbf{G_v}$	=	viscous flux
J	=	Jacobi matrix
j_i	=	electrical current density component in i direction
k	=	load factor
L	=	characteristic length scale in the paper (0.16 m)
M	=	Mach number
Pr	=	Prandtl number
p	=	statistic pressure
Res	=	Residual
R_e	=	Reynolds number
R_m	=	magnetic Reynolds number
S	=	magnetic interaction parameter
T	=	temperature
t	=	time
$\mathbf{U}$	=	conservative variables
u, v	=	velocity vector component
x, y, z	=	Cartesian coordinate direction
β_1	=	general coordinate direction
μ	=	dynamic viscosity
ξ, η, ζ	=	general coordinate direction
ρ	=	statistic density
σ	=	electrical conductivity of ionized gas
$\sim$	=	general coordinate

Subscripts

i	=	index of the grid in x direction
0	=	characteristic reference conditions
∞	=	freestream condition

Received 11 March 2010; revision received 18 May 2010; accepted for publication 20 May 2010.

*Postdoctoral Researcher; weiyi_su@nuaa.edu.cn.
†Professor, Key Laboratory of High Temperature Gas Dynamics, Institute of Mechanics. Member AIAA.
‡Professor.

I. Introduction

SHOCK-WAVE/BOUNDARY-LAYER interactions (SWBLIs) are ubiquitous in hypersonic intakes, which often result in boundary-layer separation and cause inlet flowfield distortion or even unstart. There are correlations among the onset location of boundary-layer separation point in the isolator, the momentum thickness at the scramjet inlet exit section, and the pressure at the combustor [1]. So by controlling the momentum thickness of the scramjet inlet exit section or the onset location of the separation point, the isolator can resist more backpressure in the combustor, which means much more fuel can be added into the combustor and the engine thrust increased.

Magnetohydrodynamics (MHD) is an advanced flow control method in diminishing or eliminating separation by using the Lorentz force to accelerate the boundary layer. In [2], the size of the separation bubble has been decreased about 10% by applying Lorentz force, and in [3], the velocity of the boundary-layer low-speed region is accelerated from 350 to 2000 m/s, which demonstrate the possibility and promising of MHD suppressing boundary-layer separation.

In recent years, more and more work about MHD-controlled boundary layer has been studied experimentally [4–7] and numerically [8,9]. In [8], the effects of load parameter and magnetic interaction parameter on hypersonic corner SWBLI flow has been investigated extensively. However, till to now, none of these studies has focused on how the positions of the MHD interaction zone affect SWBLI.

In this paper, a high-resolution third-order weighted ENN (essentially nonoscillatory and non-free-parameter) scheme [10,11] MHD code with low magnetic Reynolds numbers assumption has been established, with which the effects of MHD interaction-zone position on the SWBLI flow distortion, separation-bubble size, separation point location, boundary-layer velocity profile are investigated.

II. Numerical Model

A. Governing Equations

The magnetic Reynolds number shows the ratio of induced magnetic field to the applied magnetic field, MHD-controlled

boundary-layer separation belongs to low magnetic Reynolds numbers flow, so there is no need to solve the full MHD equations. The nondimensional low magnetic Reynolds MHD equations are listed as below:

$$\frac{\partial U}{\partial t}+\frac{\partial F}{\partial x}+\frac{\partial G}{\partial y}=\frac{\partial F_v}{\partial x}+\frac{\partial G_v}{\partial y}+S_{\mathrm{MHD}} \tag{1}$$

$$U=\begin{bmatrix}\rho\\ \rho u\\ \rho v\\ \rho e_t\end{bmatrix} \tag{2a}$$

$$F=\begin{bmatrix}\rho u\\ \rho u^2+p\\ \rho uv\\ (\rho e_t+p)u\end{bmatrix} \tag{2b}$$

$$G=\begin{bmatrix}\rho v\\ \rho uv\\ \rho v^2+p\\ (\rho e_t+p)v\end{bmatrix} \tag{2c}$$

$$F_v=\frac{1}{Re}\begin{bmatrix}0\\ \tau_{xx}\\ \tau_{xy}\\ u\tau_{xx}+v\tau_{xy}+q_x\end{bmatrix} \tag{2d}$$

$$G_v=\frac{1}{Re}\begin{bmatrix}0\\ \tau_{xy}\\ \tau_{yy}\\ u\tau_{xy}+v\tau_{yy}+q_y\end{bmatrix} \tag{2e}$$

$$S_{\mathrm{MHD}}=S\begin{bmatrix}0\\ j_yB_z-j_zB_y\\ j_zB_x-j_xB_z\\ E_zj_z+E_yj_y+E_xj_x\end{bmatrix} \tag{2f}$$

where

$$\tau_{ij}=\mu\left(\frac{\partial u_i}{\partial x_j}+\frac{\partial u_j}{\partial x_i}-\frac{2}{3}\frac{\partial u_k}{\partial x_k}\right) \tag{3}$$

$$e_t=\frac{p}{\rho(\gamma-1)}+\frac{1}{2}(u^2+v^2) \tag{4}$$

$$q_i=\frac{1}{(\gamma-1)M^2}\frac{\mu}{P_r}\frac{\partial T}{\partial x_i} \tag{5}$$

$$j_y=0,\qquad j_x=0,\qquad j_z=\sigma[E_z+uB_y-vB_x],\qquad S=\frac{\sigma_0B_0^2L}{\rho_\infty u_\infty} \tag{6}$$

In generalized coordinate systems, Eq. (1) becomes

$$\frac{\partial \tilde{U}}{\partial t}+\frac{\partial \tilde{F}}{\partial \xi}+\frac{\partial \tilde{G}}{\partial \eta}=\frac{\partial \tilde{F}_v}{\partial \xi}+\frac{\partial \tilde{G}_v}{\partial \eta}+\tilde{S}_{\mathrm{MHD}} \tag{7}$$

where

$$\tilde{U}=\frac{U}{J},\qquad \tilde{S}_{\mathrm{MHD}}=\frac{S_{\mathrm{MHD}}}{J} \tag{8a}$$

$$\tilde{F}=\frac{1}{J}(\xi_xF+\xi_yG),\qquad \tilde{G}=\frac{1}{J}(\eta_xF+\eta_yG) \tag{8b}$$

$$\tilde{F}_v=\frac{1}{J}(\xi_xF_v+\xi_yG_v),\qquad \tilde{G}_v=\frac{1}{J}(\eta_xF_v+\eta_yG_v) \tag{8c}$$

where J is the Jacobian of transformation. More details can be found in [10,11].

B. Solution Methods

In the paper, the inviscid flux vectors are discreted using Roe-type third-order weighted ENN schemes [10]. The conservative difference scheme of the inviscid flux vector in Eq. (7) can be written as below [10,11]:

$$\frac{\partial \tilde{F}_i}{\partial \xi}=\frac{H_{i+1/2}-H_{i-1/2}}{\Delta\xi} \tag{9}$$

$$H_{i+1/2}=H^+_{i+1/2}+H^-_{i-1/2} \tag{10}$$

$$H^+_{i+1/2}=\tilde{F}^+_i+\frac{1}{2}(\omega^+_0\Delta\tilde{F}^+_{i+1/2}+\omega^+_1\Delta\tilde{F}^+_{i-1/2})+\left(\frac{\omega^+_1}{2}-\frac{1}{6}\right)(\theta^+_0D^+_{i+1}+\theta^+_1D^+_i+\theta^+_2D^+_{i-1}) \tag{11a}$$

$$H^-_{i+1/2}=\tilde{F}^-_{i+1}-\frac{1}{2}(\omega^-_0\Delta\tilde{F}^-_{i+3/2}+\omega^-_1\Delta\tilde{F}^-_{i+1/2})+\left(\frac{\omega^-_0}{2}-\frac{1}{6}\right)(\theta^-_0D^-_{i+2}+\theta^-_1D^-_{i+1}+\theta^-_2D^-_i) \tag{11b}$$

The third term on the left in Eq. (7) can be obtained with the same method.

The viscous flux vectors of Eq. (7) are discreted with Roe-averaged central difference schemes. An explicit-implicit algorithm is also employed for Eqs. (7), i.e., the difference scheme is explicit in the ξ direction and implicit in the η direction, in which the boundary layer near the wall plays an important role.

III. Numerical Results

A. Code Validations

In this section, the supersonic conductive flows over a cylinder blunt body is computed and the shock standoff distance is compared with the analytical solution proposed by Lykoudis [12]. The computational conditions are listed in Table 1 and the computational grid is shown in Fig. 1.

Figure 2 is the relation of the shock standoff distance with the magnetic interaction parameters, where DS is the shock standoff distance at various magnetic interaction parameter S, and DS0 is the shock standoff distance without MHD-control. It can be seen that the numerical solutions are in good agreement with the analytical ones.

B. MHD-Controlled SWBLI

1. *Formulation of the Problem*

As shown in Fig. 3, the computational domain is $0 < x < 0.32$ m, $0 < y < 0.1215$ m. The flat plate is introduced from $x = 0.03$ m, in the paper, x and y are nondimensionalized with $L = 0.16$ m.

Table 1 Parameters of MHD flow over the blunt body

Property	Values
Pressure	32.3 Pa
Temperature	3708 K
Mach number	2.97
Electrical conductivity	800 mho/m
Radius of blunt body	0.025 m

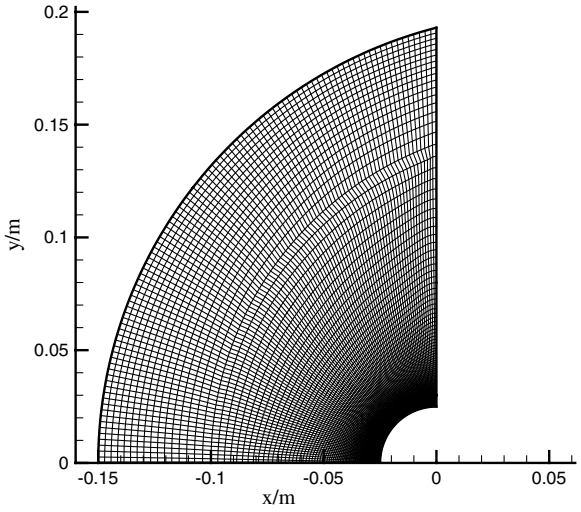

Fig. 1 Grid of MHD flows over a blunt body.

The freestream condition is $M_\infty = 2.0$, $Re = 2.96 \times 10^5$, $T_\infty = 293$ K. An oblique shock wave with 34.5° shock angle impinges on the flat plate, causing the boundary layer to separate.

Figure 3 is a sketch of MHD-controlled SWBLI boundary-layer separation. To eliminate the separation bubble, the Lorentz force should be applied to accelerate the boundary layer. In the paper, the external electrical field is applied in $-z$ direction, the external magnetic field is in y direction. For simplification, the Hall effect is neglected and the external electrical field, magnetic field, and electrical conductivity are assumed to be constant in the MHD zone. The external electrical field is given by $k = -E_z/u_\infty B_\infty$. Except for the MHD zone, the external electrical field, magnetic field, and electrical conductivity are assumed to be zero.

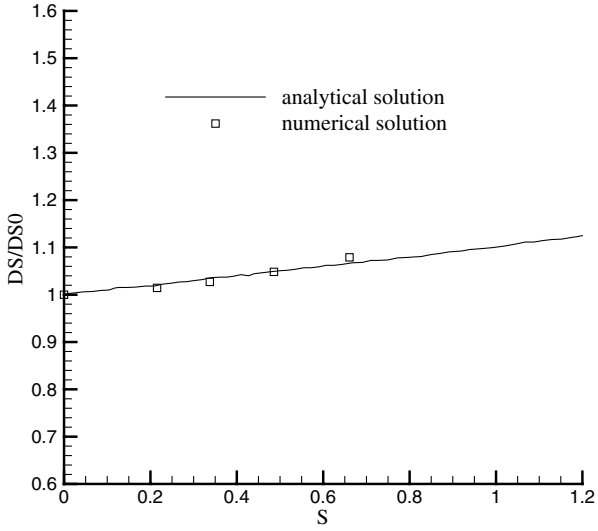

Fig. 2 Comparison of numerical solution with analytical solution of MHD flows over a blunt body.

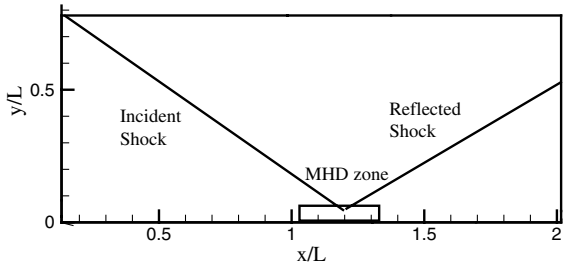

Fig. 3 Sketch of MHD-controlled SWBLI.

2. Grid Generation and Boundary Conditions

Algebraic grid generation method has been used to generate the grid. The transformation relations are

$$\xi = x \qquad \eta = 1 - \frac{\ln(\frac{\beta_1+1-y_1}{\beta_1-1+y_1})}{\ln(\frac{\beta_1+1}{\beta_1-1})} \tag{12}$$

where β_1 is a parameter that control grid distributions. $y_1 = y/h$, and h is the height of the computational domain. A grid with 256×256 has been used.

At the inflow boundary, the flowfield parameters are given by the freestream condition:

$$[\rho, \quad u, \quad v, \quad T]^T = [\rho_\infty, \quad u_\infty, \quad v_\infty, \quad T_\infty]^T \tag{13}$$

A nonslip adiabatic boundary condition is used for the bottom wall boundary condition, while the pressure is calculated using the Neumann boundary condition:

$$u = 0, \qquad v = 0, \qquad \frac{\partial T}{\partial n} = 0, \qquad \frac{\partial p}{\partial n} = 0 \tag{14}$$

For the top boundary, the freestream value is used before the incident shock wave, and the flow values after the incident shock wave are calculated used the oblique shock-wave relations.

At the outflow boundary, a two order extrapolation method is used to get the flow parameters:

$$\rho_{Nx} = \frac{4\rho_{Nx-1} - \rho_{Nx-2}}{3} \tag{15}$$

where N_x is the number of grid point in x direction, and the other flow parameter can be extrapolated in the same way.

3. Grid Sensitivity and Convergence Criteria Analysis

The effect of grid sensitivity on computational results is shown in Fig. 4. The grid density of 128×128 is 4 times that of 64×64, but the computational results change little at various grid densities.

The relative maximum density residual is shown in Fig. 5. And the relative maximum density residual Res can be expressed as

$$\text{Res} = \frac{\text{MAX}|\rho_{i,j}^{n+1} - \rho_{i,j}^{n}|}{\rho_\infty} \tag{16}$$

In Eq. (16), n is the iterative number. It can be seen from Fig. 5 that the residual occurring a peak in the range of $10,000 < N < 40,000$, showing the process of separation-bubble enlargement during shock-wave/boundary-layer interactions. And it can be found that when the iterative number exceed 50, 000, the Res < 0.0007.

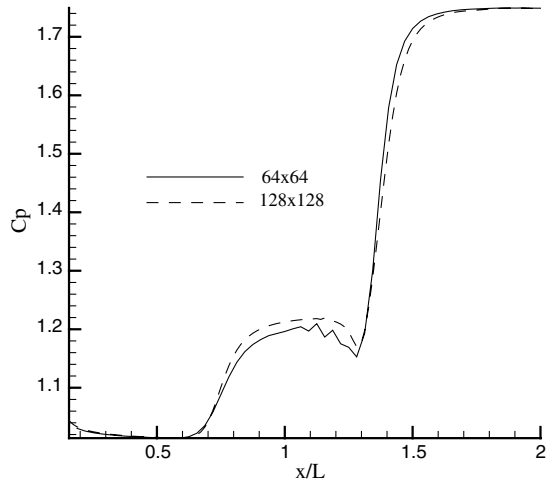

Fig. 4 Effects of grid density on wall pressure coefficients.

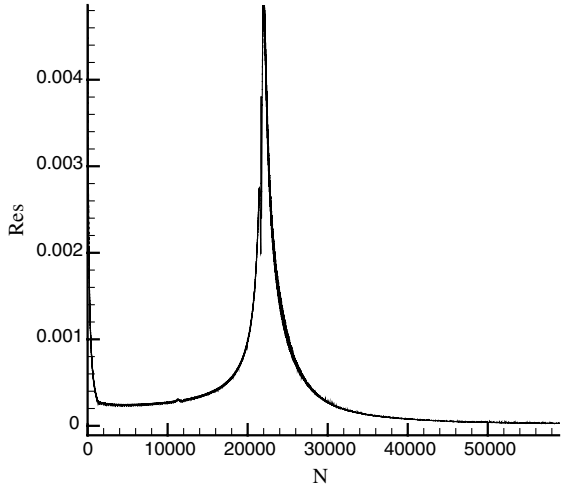

Fig. 5 Relative maximum density residual density.

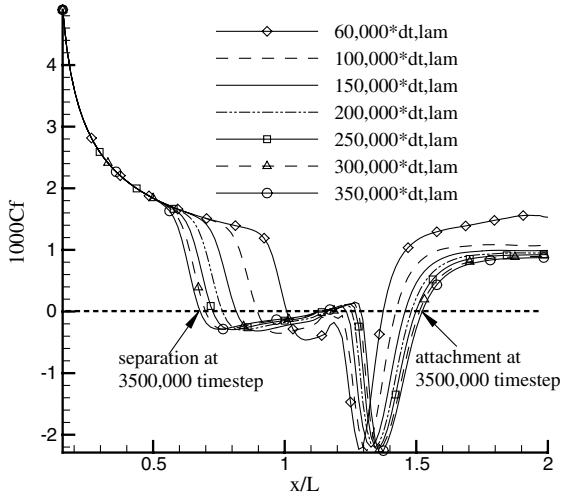

Fig. 6 Time history of shear stress for SWBLI.

4. Flowfield of SWBLI

A major characteristic of separated flows is lengthy flow establish time [13]. Figure 6 shows the characteristic property of separated flow, as the time steps increasing, the separation point moving upstream, while the reattachment point moving downstream, thus the separation bubble enlarging.

Although the establishment of SWBLI field is an unsteady process, the change of shear stress is very slowly after 250,000 time steps, which means that the steady flowfield has been established. It can be seen from Fig. 6 that when the steady field is established, the position of the separation point is $x/L = 0.5$, and the reattachment point is $x/L = 1.6$.

Table 2 Positions of MHD on SWBLI

Computational case	x_1, m	x_2, m
1	0.080	0.104
2	0.104	0.128
3	0.128	0.152
4	0.152	0.176
5	0.176	0.200
6	0.200	0.224
7	0.224	0.248
8	0.248	0.272

5. Effects of MHD Zone Position on SWBLI

The position of the MHD zone is a main factor that affects SWBLI. In this section, The SWBLI flowfields are numerically simulated with the MHD zone at different positions, and the start-point and end-point locations are listed in Table 2. The width and height of the MHD zone are $x/L = 0.15$ and $y/L = 0.015$. The load parameter is $k = 1.5$, and the magnetic interaction parameter is $S = 0.2$. In the computational cases, all the other factors are kept equal, only the position of MHD interaction zone are changed.

Figure 7 is the relation of the separation point with the location of MHD zone, where, X_{se} is the locations of the separation point with MHD-control, respectively.

It can be seen that when the location of MHD zone moves downstream the location of separation point increases first, at $x/L = 1.3$ the separation point reaches its peak values, and after the point the separation point position decreases.

The location of MHD zone also affects the position of the reattachment point. As shown in Fig. 8, the location of the reattachment point is increasing as the MHD zone moves downstream before the point $x/L = 1.3$. But the reattachment point will decrease as the MHD location continues to move downstream after this point.

Figure 9 gives the dependence of separation-bubble size to the MHD interaction-zone position. It can be put out that the separation bubble is suppressed to the minimum size when the MHD zone is at $x/L = 1.3$, which is the intersection point of incident shock with the flat plate computed with Euler equations.

The streamlines in the cases with MHD off and MHD on (case 5) are shown in Fig. 10. When the MHD is off, the separation-bubble size is about $x/L = 1.1$, and there is a secondary vortex. When the MHD is on (case 5), the secondary vortex is eliminated, and the separation size is decreased about to 50% of that without MHD-control.

The differences of separation-bubble size affect the wall pressure distributions. Figure 11 has shown some wall pressure distributions under different MHD interaction-zone positions (case 3, case 5, and case 7) listed in Table 2. In the case with MHD off, the boundary layer separates at $x/L = 0.5$, generating a separated shock wave, causing

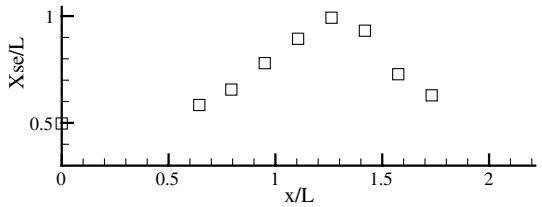

Fig. 7 Separation point vs MHD zone position.

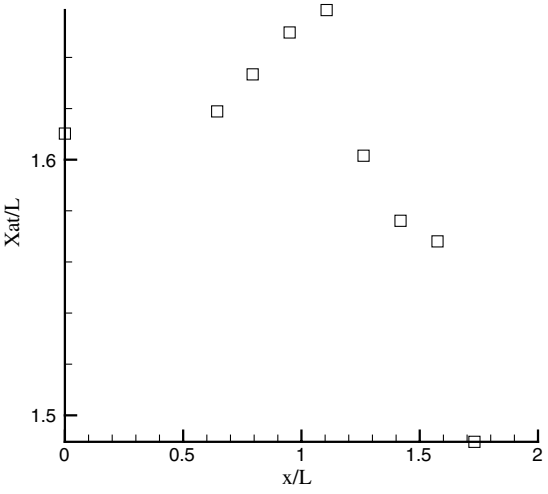

Fig. 8 Reattachment point vs MHD zone position.

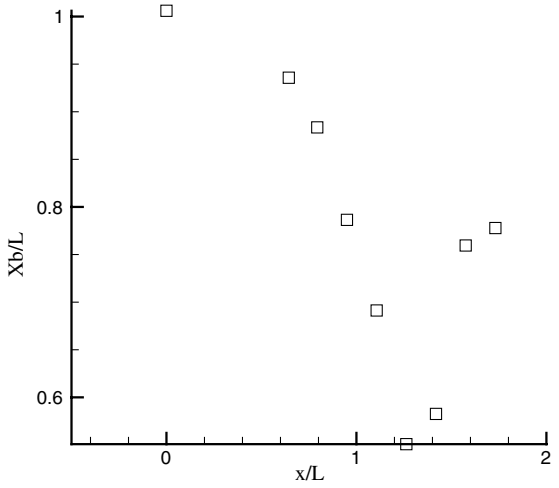

Fig. 9 Size of separation-bubble size vs MHD zone position.

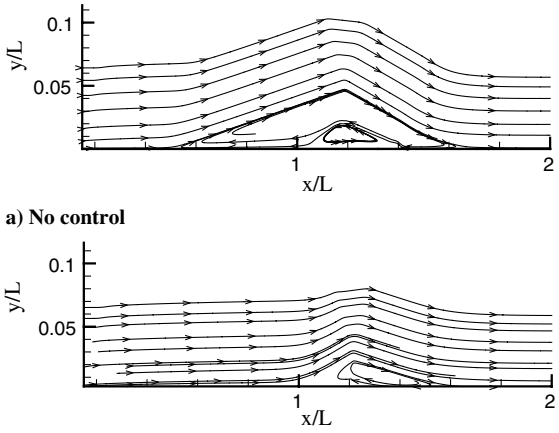

a) No control

b) MHD control (case 5)

Fig. 10 Comparison of streamlines with/without MHD control.

the wall pressure increase, and in the separation bubble, the wall pressure changes very little. The boundary layer attaches at $x/L = 1.6$, generating attach shock waves, so the pressure arises sharply.

As shown in Fig. 11, When the MHD interaction zone is before 0.152 m $< x <$ 176 m (case 5), the pressure in the separation bubble is higher than the pressure without MHD-control, while when the MHD zone position is after $0.152m < x < 176m$, the pressure is lower than the pressure without control.

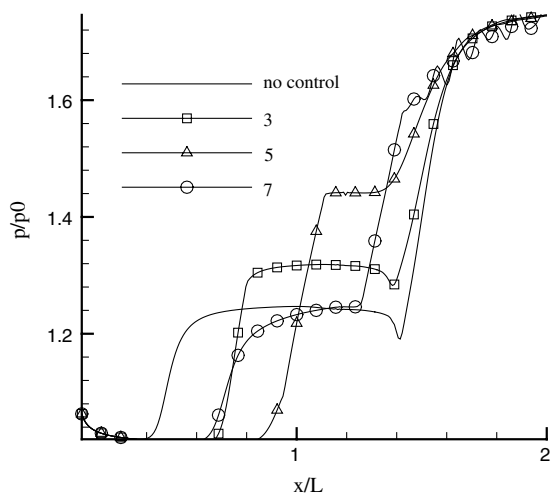

Fig. 11 Distributions of wall pressure.

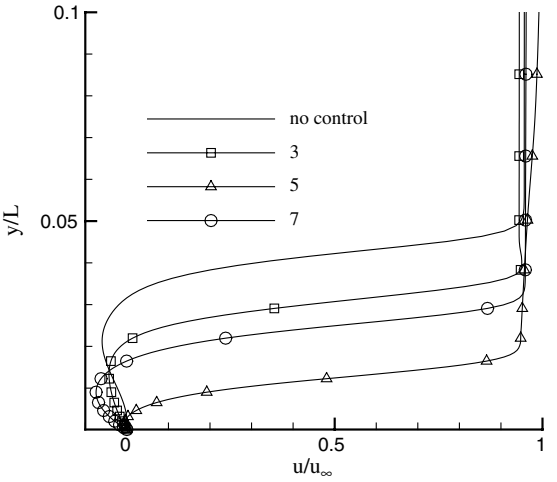

Fig. 12 Profiles of velocities ($x/L = 1.2$).

Figure 12 gives the velocity profiles at $x/L = 1.2$. It can be seen that the boundary layer is accelerated to more full compared to the case with MHD off, but the velocity profiles varies greatly with different MHD zone position. The velocities profiles is the most full When the MHD zone position is at 0.176 m $< x <$ 0.2 m (case 5). It can be found that the boundary-layer thickness decreased when the MHD is applied, and in case 5, the boundary-layer thickness is reduced to about 20% of the thickness of without MHD-control.

Figure 13 shows the profiles of temperatures at $x/L = 1.2$. It can be found that the wall temperature increases about $T/T_\infty = 0.24$ (about 70 K) in case 3 because of energy deposition in the separation bubble.

6. *Effects of MHD Zone Position on SWBLI at Different S and K*

Figure 14 gives the dependence of separation-bubble size to MHD positions when $S = 0.3$ and $k = 2$. Although the magnetic interaction parameter and load factor are different, the conclusion also shows that the best position of MHD applied is the intersection point of the incident shock wave with the flat plate.

Figure 15 gives out the relations of separation point position with MHD location. Although the separation-bubble size of MHD position at $x/L = 0.175$ is close to that of MHD position at $x/L = 0.13$, but the separation point of $x/L = 1.3$ is delayed to the farthest distance.

It can be drawn from Figs. 14 and 15 that the best position for MHD-controlling SWBLI is the intersection point of the incident

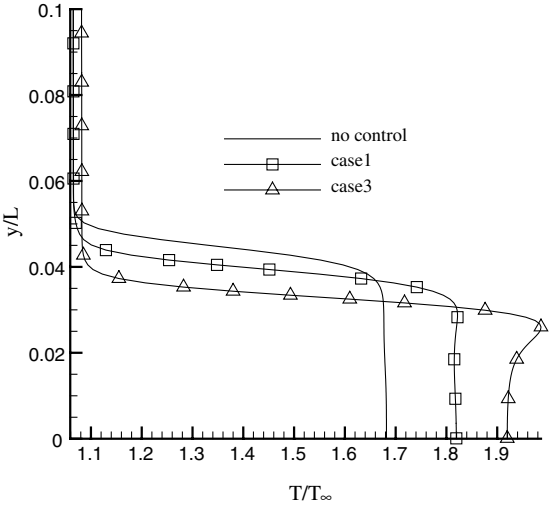

Fig. 13 Profiles of temperatures ($x/L = 1.2$).

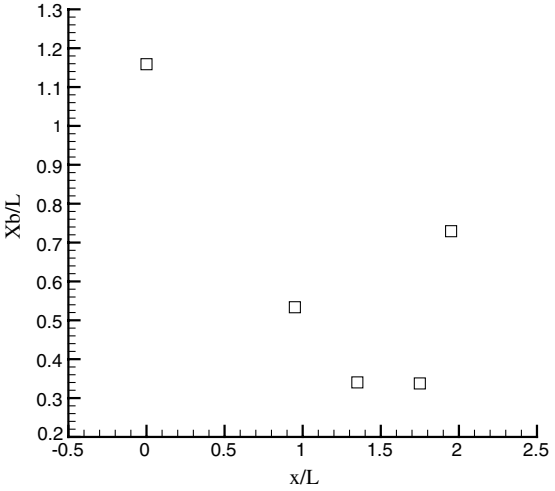

Fig. 14 Size of separation bubble vs MHD zone positions.

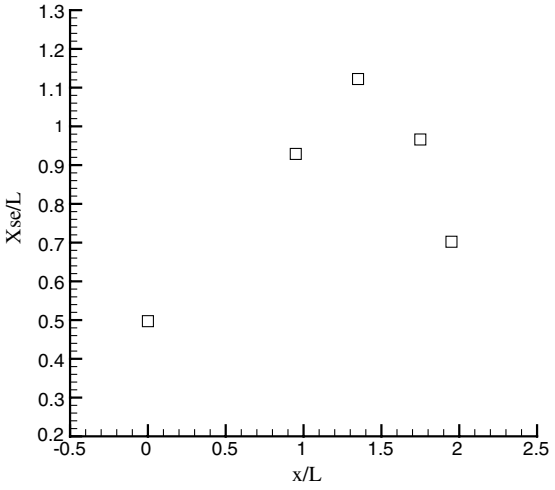

Fig. 15 Separation point vs MHD zone positions.

shock wave with the flat plate when $S = 0.3$ and $k = 2$, which corresponds well with the case of $S = 0.2$ and $k = 1.5$.

IV. Conclusions

In the present work, a two-dimensional high-order MHD code has been established, with which the effects of MHD zone position on SWBLI are investigated. The numerical results show the following:

1) The best position of MHD applied is the intersection point of the incident shock wave with the flat plate.

2) When MHD is applied at this place, the separation-bubble size is decreased up to 50% compared with the base field without control.

3) When MHD is applied at this place, the boundary-layer thickness is reduced about to 20% of the thickness without MHD-control.

The numerical simulation also demonstrates that it is possible and promising to suppress the separation bubble induced by SWBLI with MHD accelerating the boundary layer.

Acknowledgments

The work was supported by the National Natural Science Foundation of China (grant no. 90305022 and 10525212). The authors express their gratitude to Shen Yi-Qing of the Institute of Mechanics, Chinese Academy of Sciences, for his valuable advice and great help in computational fluid dynamics code.

References

[1] Waltrup, P. J., and Billig, F. S., "Structure of Shock Wave in Cylindrical Ducts," *AIAA Journal*, Vol. 11, No. 10, 1973, pp. 1404–1408. doi:10.2514/3.50600

[2] Udagawa, K., Kaminaga, S., and Asano, H., "MHD Boundary Layer Flow Acceleration Experiments," AIAA Paper 2006 -3233, June 2006.

[3] Zaidi, S. H., Smith, T., Macheret, S. O., and Miles, R. B., "Snowplow Surface Discharge in Magnetic Field for High Speed Boundary Layer Control," AIAA Paper 2006-1006, Jan. 2006.

[4] Kalra, C. S., Shneider, M. N., and Miles, R. B., "Numerical Study of Shockwave Induced Boundary Layer Separation Control Using Plasma Actuators," AIAA Paper 2008-1095, Jan. 2008.

[5] Kalra, C., Zaidi, S. H., Alderman, B. J., and Miles, R. B., "Non-Thermal Control of Shock-Wave Induced Boundary Layer Separation Using Magneto-Hydrodynamics," AIAA Paper 2007-4138, June 2007.

[6] Kalra, C., Zaidi, S. H., Alderman B. J., Miles, R. B., and Murty, Y.V., "Magnetically Driven Surface Discharges for Shock-Wave Induced Boundary-Layer Separation Control," AIAA Paper 2007-222, Jan. 2007.

[7] Saito, S., Udagawa, K., Kawaguchi, K., Tomioka, S., and Yamasaki, H., "Boundary Layer Separation Control by MHD Interaction," AIAA Paper 2008-1091, Jan. 2008.

[8] Kalra, C. S., Shneider, M. N., and Miles, R. B., "Numerical Study of Boundary Layer Separation Control Using Magnetohydrodynamic Actuators," *Physics of Fluids*, Vol. 21, No. 10, 2009, Paper 106101. doi:10.1063/1.3233658

[9] Updike, G. A., Shang, J. S., and Gaitonde, D. V., "Hypersonic Separated Flow Control Using Magneto-Aerodynamic Interaction," AIAA Paper 2005-164, Jan. 2005.

[10] Wang, R. Q., and Shen, Y. Q., "Some Weight-Type High-Resolution Difference Schemes and Their Applications," *Acta Mechanica Sinica*, Vol. 15, No. 4, 1999, pp. 313–324. doi:10.1007/BF02487929

[11] Shen, Y. Q., Wang, R. Q., and Liao, H. Z., "A New Numerical Study of the Shock/Boundary-Layer Interaction," *International Journal for Numerical Methods in Fluids*, Vol. 33, No. 1, 2000, pp. 23–34. doi:10.1002/(SICI)1097-0363(20000515)33:1<23::AID-FLD980>3.0.CO;2-B

[12] Lykoudis, P. S., "The Newtonian Approximation in Magnetic Hypersonic Stagnation-Point Flow," *Journal of the Aero/Space Sciences*, Vol. 28, No. 7, 1961, pp. 541–546.

[13] Abraham, G. A., "The Effects of Surface Catalysis on the Hypersonic Shock/Boundary Layer Interaction," Ph.D. Dissertation, Univ. of Maryland, College Park, MD, 1994, p. 98.

C. Segal
Associate Editor